Featured in Physics

Coherent Coupling between Phonons, Magnons, and Photons

Zhen Shen,[1,2,*] Guan-Ting Xu,[1,2,*] Mai Zhang,[1,2,*] Yan-Lei Zhang,[1,2] Yu Wang,[1,2] Cheng-Zhe Chai,[3] Chang-Ling Zou,[1,2,4] Guang-Can Guo,[1,2,4] and Chun-Hua Dong[1,2,4,†]

[1]*CAS Key Laboratory of Quantum Information, University of Science and Technology of China, Hefei 230026, People's Republic of China*

[2]*CAS Center for Excellence in Quantum Information and Quantum Physics, University of Science and Technology of China, Hefei, Anhui 230026, People's Republic of China*

[3]*Yongjiang Laboratory (Y-LAB), Ningbo, Zhejiang 315202 People's Republic of China*

[4]*Hefei National Laboratory, University of Science and Technology of China, Hefei, Anhui 230088, People's Republic of China*

(Received 22 July 2022; revised 25 October 2022; accepted 4 November 2022; published 9 December 2022)

Mechanical degrees of freedom, which have often been overlooked in various quantum systems, have been studied for applications ranging from quantum information processing to sensing. Here, we develop a hybrid platform consisting of a magnomechanical cavity and an optomechanical cavity, which are coherently coupled by the straightway physical contact. The phonons in the system can be manipulated either with the magnetostrictive interaction or optically through the radiation pressure. Together with mechanical state preparation and sensitive readout, we demonstrate the microwave-to-optical conversion with an ultrawide tuning range up to 3 GHz. In addition, we observe a mechanical motion interference effect, in which the optically driven mechanical motion is canceled by the microwave-driven coherent motion. Manipulating mechanical oscillators with equal facility through both magnonic and photonic channels enables new architectures for signal transduction between the optical, microwave, mechanical, and magnetic fields.

DOI: 10.1103/PhysRevLett.129.243601

Introduction.—A variety of quantum systems including both atomic and solid state systems, such as rare-earth-ion-doped crystals, superconducting circuits, and spins in yttrium iron garnet (YIG) or diamond, have emerged as promising candidates for matter qubits [1–5]. Different quantum systems make them suitable for specific quantum operations. A universal approach about cavity optomechanics for manipulating interactions between different types of quantum systems emerged recently for incorporating and taking advantage of disparate quantum systems [6–10], i.e., a hybrid quantum network to enable quantum communication between these systems [11,12]. Particularly, magnetostrictive force [13,14], radiation force [15,16], electrostatic force [9,17,18], and piezoelectric force [8,19–21] have been used for coupling mechanical motion with magnons and optical or microwave photons. The ubiquitous nature of mechanical motion can enable a macroscopic mechanical oscillator to couple nearly any type of quantum systems, including charge, spin, atomic, and superconducting qubits, as well as to photons at nearly any wavelength [1,3,11,22].

Such interaction mechanisms lead to the fast development of cavity magnomechanical and optomechanical systems having their respective advantages. Especially, because of the great tunability of magnons [23,24], the microwave-to-optical conversion with an ultrawide tuning range up to 2.5 GHz has been demonstrated in an optomagnonic system [25]. However, current implementation of cavity optomagnonics remains orders of magnitude larger in volume and smaller Q factor in optical modes than state-of-the-art cavity optomechanical devices, resulting in limited magneto-optical interaction strength [26–31]. In contrast, benefiting from the higher Q factor to enhance the interactions, most optomechanical systems intrinsically lack tunability, limiting their practical applications [17–21,32–34].

Here, we develop a platform consisting of an optomechanical cavity (silica microsphere) and a magnomechanical cavity (YIG microsphere), which are coherently coupled by the straightway physical contact. The mechanical motions in the distinct resonators are explored by the radiation pressure based on the circulating optical fields or the magnetostrictive force through microwave-driven magnons. Then, the microwave-excited mechanical motion acts as a phonon source for the breathing mode of optomechanical resonator, and phase-sensitive optical measurements confirm the ability to initialize the mechanical oscillator with the desired amplitude and phase. The microwave-to-optical conversion is demonstrated in such magno-optomechanical hybrid system with an ultrawide tuning range up to 3 GHz. In addition, we observe a mechanical motion interference, in which the optically induced motion of the mechanical resonator is canceled by microwave-driven coherent motion, and vice versa. This demonstration

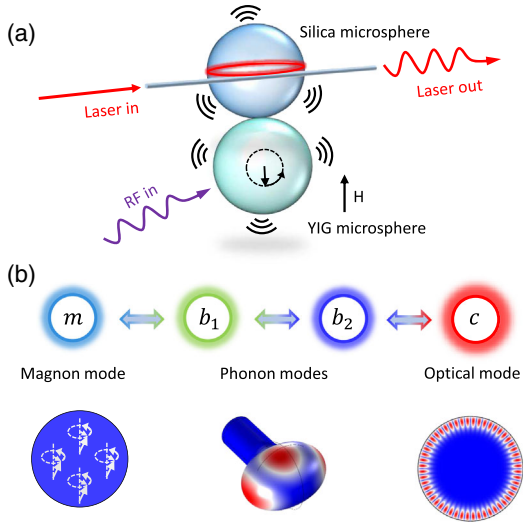

FIG. 1. (a) Schematic of the device that consists of a YIG and a silica microsphere, which both support the mechanical modes excited by the magnetostrictive interaction through magnons or the radiation pressure induced by the circulating optical fields. Based on the straightway physical contact, the localized mechanical modes establish direct coupling. (b) Schematic of the coupling between magnons, phonons, and photons and an intuitive illustration of the magnon, phonon, and photon mode.

of a hybrid platform that combines controlled phonons, magnons, and photons will enable new applications of signal transduction and sensing.

Coupling between the localized mechanical modes: The device used in our experiment, including the key components of the single-crystal YIG microsphere and silica microsphere, is schematically shown in Fig. 1(a). The YIG microsphere supports a uniform magnon mode with an external magnetic field H, and the magnon can couple with mechanical modes through magnetostrictive interaction [13,14], which allows us to excite phonons in YIG microsphere by microwaves. Meanwhile the optical and mechanical modes in the silica microcavity can be coupled through radiation pressure and photoelastic effect [7,35]. Because of the direct contact of the microcavities, the localized mechanical modes establish direct coupling, which also induces the interaction between the magnons and photons. Our system enables new architectures for signal transduction between the optical, microwave, and mechanical domains based on coherent coupling between photons, phonons, and magnons, as shown in Fig. 1(b). Considering the interaction in our system, the Hamiltonian is given as

$$\begin{aligned} H = {} & \omega_m m^\dagger m + \omega_{b_1} b_1^\dagger b_1 + \omega_{b_2} b_2^\dagger b_2 + \omega_c c^\dagger c \\ & + g_{\mathrm{mp}}(b_1^\dagger + b_1) m^\dagger m + g_{\mathrm{pp}}(b_1^\dagger b_2 + b_2^\dagger b_1) \\ & + g_{\mathrm{po}}(b_2^\dagger + b_2) c^\dagger c, \end{aligned} \tag{1}$$

where m, $b_{1(2)}$, and c are the annihilation operators of the magnon, the localized mechanical modes in YIG and silica microspheres, and the optical mode, with the angular frequency of ω_m, $\omega_{b_1(b_2)}$, and ω_c, respectively. g_{mp}, g_{pp}, and g_{po} are the single excitation coupling rate for magnon-phonon, phonon-phonon, and phonon-photon interactions, respectively (see Supplemental Material [36]).

The experiment setup is illustrated in Fig. 2(a). The optical modes near 1550 nm in the silica microsphere with a diameter of about 200 μm are excited through the evanescent field of a tapered fiber. Figure 2(b) shows the transmission of the optical mode used in the experiment, which has a dissipation rate of $\gamma_c/2\pi = 10$ MHz, corresponding to a loaded Q factor of 1.9×10^7. Since the contact surface is far away from the evanescent field of optical mode, the high-Q factor is maintained. Actually, two mechanical modes b_2 and b_3 with the frequency of $\omega_{b_2}/2\pi = 15.186$ MHz and $\omega_{b_3}/2\pi = 15.367$ MHz are observed in such a microsphere, as shown in Fig. 2(c). The intrinsic dissipation rates of two mechanical modes are $\gamma_{b_2}/2\pi = 1$ kHz and $\gamma_{b_3}/2\pi = 6.4$ kHz, respectively.

To match the mechanical frequency in the silica microsphere, a 200-μm-diameter YIG microsphere is used. The magnon mode excited by an antenna is the uniform mode as known as Kittel mode, whose frequency of $\omega_m/2\pi = 4.805$ GHz determined by the gyromagnetic ratio and the external bias magnetic field H [25,39]. Figure 2(d) shows the magnon resonance through the microwave reflection spectrum S_{11} obtained by a vector network analyzer (VNA), corresponding to a dissipation rate of $\gamma_m/2\pi = 1$ MHz. When a microwave is around the magnon resonance, the mechanical mode can be excited even two microcavities contact together, as shown in Fig. 2(f). The frequency of the mechanical mode is $\omega_{b_1}/2\pi = 15.25$ MHz with a dissipation rate $\gamma_{b_1}/2\pi = 5.2$ kHz, which is damped from 3.2 kHz. Meanwhile the decay rates of phonon modes b_2 (b_3) degenerates to $\gamma_{b_2}/2\pi = 1.9$ kHz ($\gamma_{b_3}/2\pi = 8$ kHz) (see Supplemental Material [36]).

Considering the inevitable frequency mismatch between the magnon and phonon modes with our experimental parameters, a strong microwave drive (∼76 mW) is used to compensate for their frequency difference [13]. This is a three-wave mixing process, where two photons (drive photon and signal photon) and one phonon interact with each other. Thus, the frequency of the three modes should satisfy the energy conservations [40]. Here, the microwave drive (ω_d) is fixed at one mechanical frequency (ω_{b_1}) below the magnon resonance, as shown in Fig. 2(e). It would lead to coherent conversion between magnon and phonon when a microwave signal (ω_s) is scanning through the magnon resonance and induce a sharp transparency window of the spectra S_{11} when the detuning $\delta = \omega_s - \omega_d$ equals to ω_{b_1} [13]. The transparency window originates from the destructive interference between the signal field

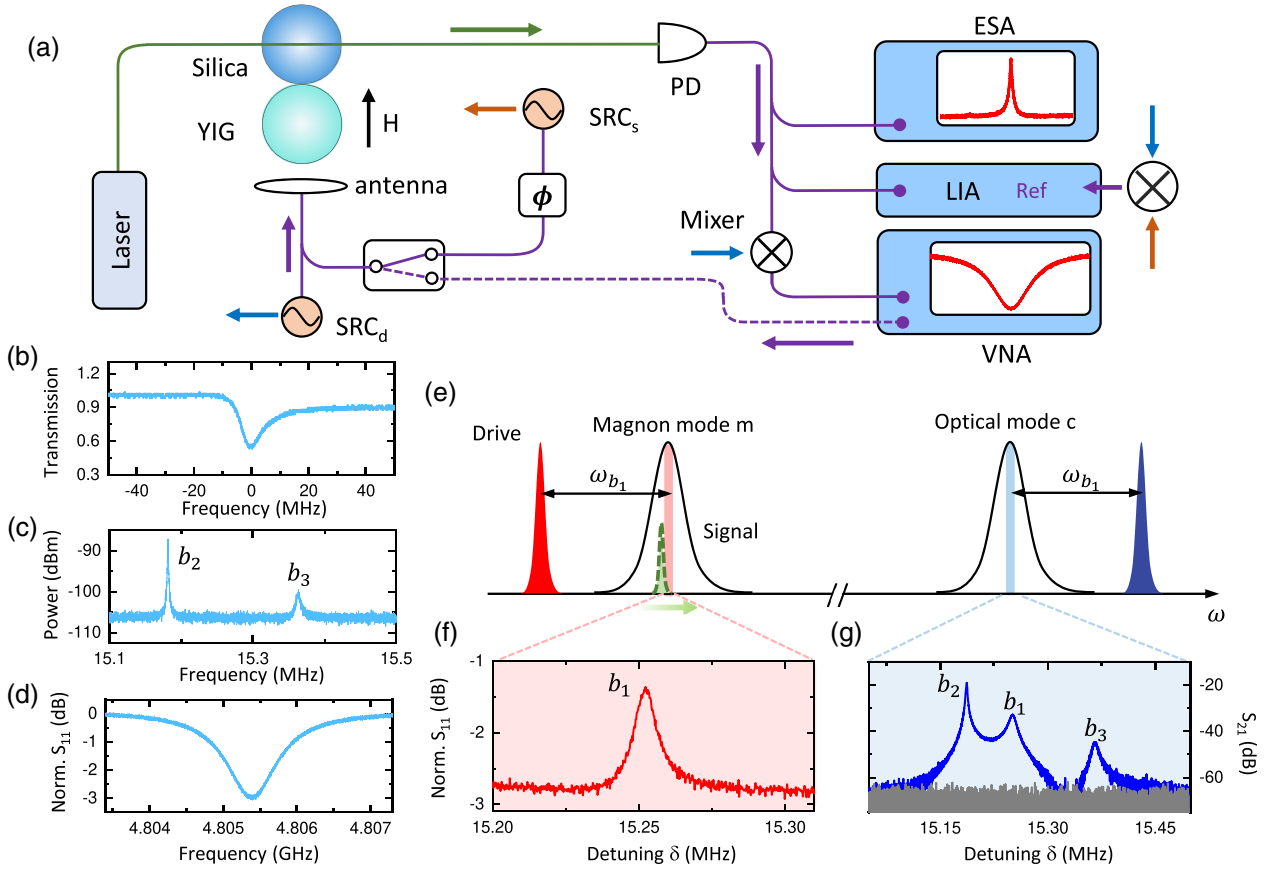

FIG. 2. Coupling between the localized mechanical modes. (a) The measurement setup. Green lines represent optical paths, and purple, blue, and orange lines represent electrical connections. ESA, electrical spectrum analyzer; LIA, lock-in amplifier; VNA, vector network analyzer; SRC, microwave source; PD, photodetector; ϕ, phase shifter. (b) Optical transmission spectrum for the optical mode c in the silica microsphere. (c) Displacement power spectrum of the two radial breathing modes in the single silica microsphere. (d) Measured microwave reflection spectrum of the magnon mode m. (e) Spectral diagram of the coherent coupling between magnons, phonons, and microwave and optical photons. (f) Measured reflection spectrum when a microwave signal is swept across the magnon mode resonance with a strong microwave drive (76 mW), which is red detuned from the magnon mode m with the detuning $\Delta_d = \omega_d - \omega_m = -\omega_{b_1}$. (g) Microwave-driven mechanical motion spectrum S_{21} obtained from the optical probing of the silica microsphere when two microcavities contacted (blue) or separated (gray).

and the microwave field generated from the anti-Stokes scattering process, as shown in Fig. 2(f). For sensitive detection of the mechanical motion in the YIG microsphere, we use the high-Q optical mode in the silica microsphere for optical readout. The VNA drives the magnon and reads out the coherent component of the photodetected signal S_{21}. Figure 2(g) shows the measured S_{21}, including three peaks above the background (blue), which are, respectively, corresponding to the mechanical modes in the YIG and silica microcavities. In contrast, the three peaks will disappear (gray) when two microcavities spatially separated, indicating no coupling between the mechanical modes. The coupling strength $g_{\rm pp}$ is determined by the contact regime of the vibration modes [41]. Although the microwave drive would induce heat to cause the frequency shift of magnon and optical modes, they can be compensated by changing the magnon resonance via the bias magnetic field and by tuning the laser frequency, respectively. And the off-resonance microwave drive ($|\omega_d - \omega_m| \gg \gamma_m$) does not produce excessive intracavity power, and our system with the strong microwave drive is still stable. As a proof of principle, mode b_2 with a smaller decay rate is chosen for microwave-to-optical conversion and mechanical motion interference in the following experiments, while mode b_3 owning equal feasibility is used to demonstrate the mechanical state preparation and readout [Figs. 3(a) and 3(b)].

Coherent mechanical motion and microwave-to-optical conversion: For coherent control of the mechanical motion, we need to transfer both the rf amplitude and phase onto the optical cavity displacement. The frequency of the microwave signal is fixed at 4.8054 GHz, so that the frequency difference with the microwave drive resonates with phonon mode b_3 to excite the coherent mechanical motion. We measure the photodetected signal by a lock-in amplifier, where the difference frequency between the

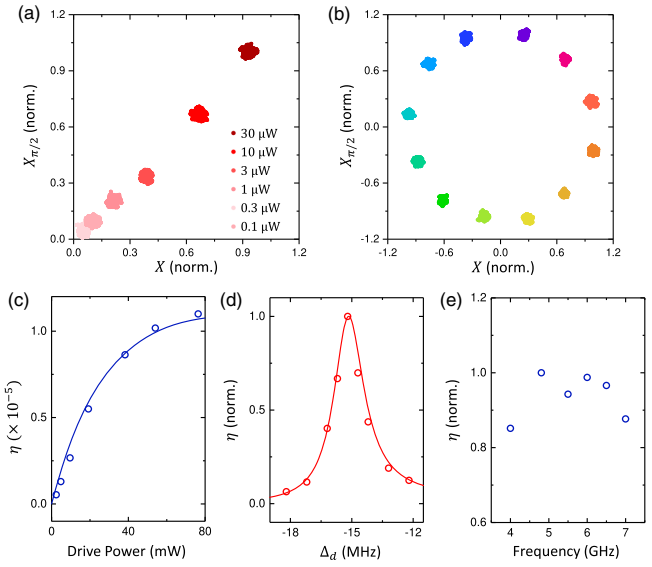

FIG. 3. Coherent mechanical motion and microwave-to-optical conversion. (a) Quadrature distributions of the mechanical state with increasing the microwave signal power. (b) Quadrature measurement of the coherent mechanical state with varying phase. (c) The microwave-to-optical conversion efficiency as a function of the microwave drive power. (d) The normalized conversion efficiency versus drive-resonance detunings Δ_d. (e) The conversion efficiency as a function of the microwave signal frequency (normalized to the efficiency of 4.8 GHz). The signal-drive detuning and drive-resonance detuning are maintained $\Delta_{sd} = -\Delta_d = \omega_{b_2}$.

microwave signal and the drive is used as the local oscillator. Figure 3(a) shows the in-phase and quadrature components of the photodetected signal (X, $X_{\pi/2}$) on resonance for different displacements of mechanical motion, via varying the power of microwave signal applied to the magnon mode. Figure 3(b) shows the data plotted against the phase of microwave signal. These results show that the mechanical modes of the YIG and silica microspheres can achieve coherent coupling through physical contact, and the mechanical state with arbitrary amplitude and phase can be prepared through magnetostrictive interaction.

When the laser drive is fixed at one mechanical frequency below the cavity resonance, the optomechanical interaction can convert the coherent phonons into photons, thus achieving microwave-to-optical conversion. Here, we fix the frequency of microwave signal to convert the phonon mode b_2 ($\omega_s = \omega_d + \omega_{b2}$) and the power of optical carrier. Figure 3(c) plots the conversion efficiency as a function of the microwave drive power. As the microwave drive power increases, the enhancement of the magnomechanical interaction leads to stronger mechanical motion and higher conversion efficiency. The maximum conversion efficiency achieved in the experiment is approximately 1.1×10^{-5} (see Supplemental Material [36]). Figure 3(d) shows measured conversion efficiency for drive-resonance detunings $\Delta_d = \omega_d - \omega_m$ varying from -12.2 to -18.2 MHz, which can be achieved only by changing the bias magnetic field to tune the magnon resonance ω_m. The conversion efficiency is normalized to the value of $\Delta_d = -\omega_{b_2}$. The spectra agree with the theoretical predictions of the steady-state intracavity field:

$$c^\dagger = \frac{iG^*_{\mathrm{MO}}\sqrt{\kappa_{m,\mathrm{ex}}}\mathcal{E}_{S,M}}{\gamma_{\mathrm{MO}}(1+C_{\mathrm{MO}})}, \tag{2}$$

where $G_{\mathrm{MO}} = G_{\mathrm{mp}} g_{\mathrm{pp}} G_{\mathrm{po}}$ is the effective coupling strength, with $G_{\mathrm{mp}} = \sqrt{N_{\mathrm{dm}}} g_{\mathrm{mp}}$ and $G_{\mathrm{po}} = \sqrt{N_{\mathrm{dc}}} g_{\mathrm{po}}$. N_{dm} and N_{dc} are the intracavity magnon and photon number of the driving fields, respectively. $\gamma_{\mathrm{MO}} = [-\gamma_m/2 + (\tilde{\gamma_{b_2}}/2 |G_{\mathrm{mp}}|^2/\gamma_{b_1}\tilde{\gamma_{b_2}}/4 + g_{\mathrm{pp}}^2)][-\tilde{\gamma_c}/2 - (-\gamma_{b_1}/2|G_{\mathrm{po}}|^2/\gamma_{b_1}\tilde{\gamma_{b_2}}/4 + g_{\mathrm{pp}}^2)](\gamma_{b_1}\tilde{\gamma_{b_2}}/4 + g_{\mathrm{pp}}^2)$ is the effective dissipation rate, with $\tilde{\gamma_{b2}}/2 = i(\omega_{b_1} - \omega_{b_2}) - \gamma_{b_2}/2$ and $\tilde{\gamma_c}/2 = i(\omega_{b_1} - \omega_{b_2}) - \gamma_c/2$. $C_{\mathrm{MO}} = -|G_{\mathrm{MO}}|^2/[\gamma_{\mathrm{MO}}(\gamma_{b_1}\tilde{\gamma_{b_2}}/4 + g_{\mathrm{pp}}^2)]$ is the effective cooperativity; $\mathcal{E}_{S,M}$ is the signal amplitude of external microwave field. In Eq. (2), when microwave drive power is 76 mW, $|C_{\mathrm{MO}}| = 6.42 \times 10^{-4}$, $|G_{\mathrm{MO}}|/(2\pi)^3 = 2.19 \times 10^{15}$ Hz^3, and $|\gamma_{\mathrm{MO}}|/(2\pi)^4 = 7.16 \times 10^{23}$ Hz^4. Since the external magnetic field can tune the frequency of the magnon, we can realize 4–7 GHz microwave conversion by tuning the magnon frequency and the relevant microwave drive to match drive-resonance detuning $\Delta_d = -\omega_{b_2}$, as shown in Fig. 3(e). Although a single YIG microcavity has been used to study the magnon-phonon and direct magnon-photon interactions [13,26], which allows the microwave-to-optical conversion, the conversion efficiency can be enhanced to around 10^7-fold using our phonon-mediated magnon-photon coupling. Theoretical analysis shows the conversion efficiency can be greatly improved by reducing the frequency difference $\Delta_b = \omega_{b_2} - \omega_{b_1}$ (see Supplemental Material [36]).

Mechanical motion interference: We have shown that mechanical motion driven by a magnon can effectively transfer to the localized mechanical mode of a silica microcavity. In other word, the mechanical resonator could be simultaneously excited using both magnons and optical fields. Therefore, a mechanical motion interference effect could occur between two pathways, as shown in Fig. 4(a). One is excited through microwave-driven magnons, and the other one is parametric down-conversion from the optical signal on the resonant cavity mode with the mechanical interaction when a control laser is driven at one mechanical frequency above the cavity resonance. The phonons in two pathways can be independently adjusted to have arbitrary even opposite phases, inducing the mechanical motion suppression. Figure 4(b) presents the experimental setup, where the optical signal is generated from the modulated strong driving laser. The rf signals drive the magnon and down-convert to drive the electro-optic phase modulator for optically stimulating the phonons. The signal of the

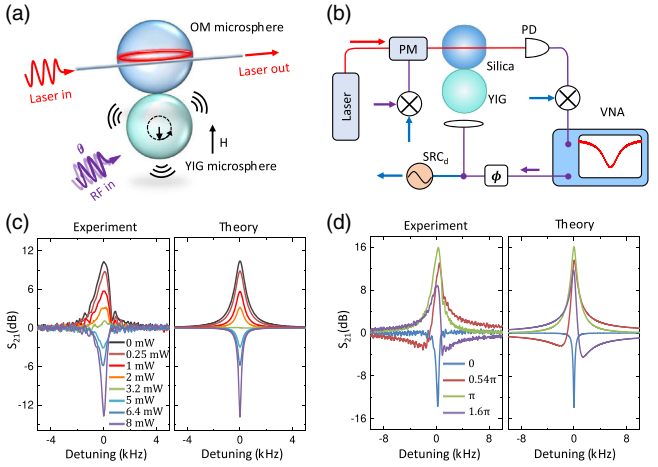

FIG. 4. Mechanical motion interference. (a) Schematic indicating a mechanical motion interference. (b) The measurement setup. While part of the VNA output is sent to the magnon for microwave-driven mechanical motion in YIG microsphere, it is also down-converted to drive the electro-optic phase modulator (PM) for optically stimulating the phonons in silica microsphere. (c) The S_{21} spectra as increasing the microwave drive power, implying the evolution of mechanical motion from optomechanical drive dominated to microwave drive dominated (from black to purple lines). (d) The S_{21} spectra by varying only the phase of rf signal applied to the magnon mode and fixing both rf drive and signal power, giving rise to peak (dip) and asymmetric Fano line shapes.

photodetector (PD) is up-converted and fed into the VNA for the measurement of S_{21}.

Figure 4(c) shows a series of S_{21} spectra obtained by the VNA as the rf drive power is increased, corresponding to changing the phonons in the YIG microsphere. The top black lines in Fig. 4(c) represent the typical optomechanically induced amplification spectra when the microwave drive turned off [42]. By increasing the rf drive power and adjusting the phase of VNA output to destructive interference, the peak is gradually reduced and eventually disappeared, as shown green lines in Fig. 4(c). This means that both the optomechanically induced mechanical motion and modulated spectrum are completely canceled. When the rf drive power continues to increase, the displacement amplitude of the silica microcavity will start to increase from zero and is dominated by the energy transferred from the YIG mechanical motion (purple lines). As we expected, due to the reversal phase of mechanical motion, the peak in spectra is gradually converted to a dip [42]. Experimental results shown in Fig. 4(c) agree with the theoretical result that

$$c^{\dagger} = \frac{\frac{iG^{*}_{\mathrm{MO}}\sqrt{\kappa_{m,\mathrm{ex}}}}{(\chi_{b_1}\chi_{b_2}+g^{2}_{\mathrm{pp}})}\mathcal{E}_{S,M}e^{i\theta} - \tilde{\chi}_m\sqrt{\kappa_{c,\mathrm{ex}}}\mathcal{E}_{S,O}}{\tilde{\chi}_m\tilde{\chi}_c - |G_{\mathrm{MO}}|^2/(\chi_{b_1}\chi_{b_2}+g^{2}_{\mathrm{pp}})^2}. \tag{3}$$

Here, $\chi_{b_1} = i\delta_1 - \gamma_{b_1}/2$ and $\chi_{b_2} = i(\delta_1 - \Delta_b) - \gamma_{b_2}/2$, where $\delta_1 = \omega_{S,M} - \omega_m$ is the signal-resonance detuning and $\Delta_b = \omega_{b_2} - \omega_{b_1}$ is the frequency difference between two phonon modes. $\tilde{\chi}_m = (i\delta_1 - \gamma_m/2) + (\chi_{b_2}|G_{\mathrm{mp}}|^2/\chi_{b_1}\chi_{b_2+g^2_{\mathrm{pp}}})$ and $\tilde{\chi}_c = [i(\delta_1 - \Delta_b) - \gamma_c/2] - (\chi_{b_1}|G_{\mathrm{po}}|^2/\chi_{b_1}\chi_{b_2+g^2_{\mathrm{pp}}})$. $\kappa_{c,\mathrm{ex}}$ is the external coupling rate between microfiber and silica microsphere. $\mathcal{E}_{S,O}$ is the signal amplitude of optical field. In Eq. (3), when microwave drive power is 8 mW, $|C_{\mathrm{MO}}| = 1.08 \times 10^{-4}$, $|G_{\mathrm{MO}}|/(2\pi)^3 = 7.11 \times 10^{14}$ Hz^3, and $|\gamma_{\mathrm{MO}}|/(2\pi)^4 = 1.08 \times 10^{24}$ Hz^4. Figure 4(d) shows the S_{21} spectrum by varying only the phase of rf signal applied to the magnon mode and fixing both rf drive and signal power, corresponding to varying the phase of the phonon. The spectra of S_{21} are obviously changed, giving rise to a peak (dip) and asymmetric Fano line shapes. Since the mechanical displacement excited by the magnons is 1.2 times larger than that excited by optical fields, it does not exhibit complete destructive interference.

In summary, we have presented a magno-optomechanical platform in which a magnomechanical cavity is in physical contact with an optomechanical cavity. Several effects have been demonstrated, including the mechanical state sensitive readout and preparation with desired amplitude and phase, microwave-to-optical conversion with tuning range up to 3 GHz, and the mechanical motion interference effect. Considering the easily reached strong magnon-photon coupling in microwave cavities, phonon manipulation and microwave-to-optical conversion can be achieved with lower power consumption. Our hybrid platform will find applications in various fields, such as tunable slow light or delay lines in both microwave and optical domains [35,43], and quantum signal transduction and sensing for quantum networks [12,44,45].

The work was supported by the National Key R&D Program of China (Grant No. 2020YFB2205801), Innovation program for Quantum Science and Technology (2021ZD0303203), the National Natural Science Foundation of China (Grants No. 11934012, No. 11874342, and No. 92050109), University of Science and Technology of China (USTC) Research Funds of the Double First-Class Initiative (YD2470002002), and the Fundamental Research Funds for the Central Universities. C.-H. D. was supported the State Key Laboratory of Advanced Optical Communication Systems and Networks, Shanghai Jiao Tong University, China. This work was partially carried out at the USTC Center for Micro and Nanoscale Research and Fabrication.

*These authors contributed equally to this work.
†chunhua@ustc.edu.cn

[1] X. Liu, J. Hu, Z.-F. Li, X. Li, P.-Y. Li, P.-J. Liang, Z.-Q. Zhou, C.-F. Li, and G.-C. Guo, Heralded entanglement distribution between two absorptive quantum memories, Nature (London) **594**, 41 (2021).

[2] N. Ofek, A. Petrenko, R. Heeres, P. Reinhold, Z. Leghtas, B. Vlastakis, Y. Liu, L. Frunzio, S. Girvin, L. Jiang *et al.*, Extending the lifetime of a quantum bit with error correction in superconducting circuits, Nature (London) **536**, 441 (2016).

[3] M. Mirhosseini, A. Sipahigil, M. Kalaee, and O. Painter, Superconducting qubit to optical photon transduction, Nature (London) **588**, 599 (2020).

[4] S. Klingler, V. Amin, S. Geprägs, K. Ganzhorn, H. Maier-Flaig, M. Althammer, H. Huebl, R. Gross, R. D. McMichael, M. D. Stiles, S. T. B. Goennenwein, and M. Weiler, Spin-Torque Excitation of Perpendicular Standing Spin Waves in Coupled YIG/Co Heterostructures, Phys. Rev. Lett. **120**, 127201 (2018).

[5] S. Maity, B. Pingault, G. Joe, M. Chalupnik, D. Assumpção, E. Cornell, L. Shao, and M. Lončar, Mechanical Control of a Single Nuclear Spin, Phys. Rev. X **12**, 011056 (2022).

[6] M. Aspelmeyer, P. Meystre, and K. Schwab, Quantum optomechanics, Phys. Today **65**, No. 7, 29 (2012).

[7] M. Aspelmeyer, T. J. Kippenberg, and F. Marquardt, Cavity optomechanics, Rev. Mod. Phys. **86**, 1391 (2014).

[8] J. Bochmann, A. Vainsencher, D. D. Awschalom, and A. N. Cleland, Nanomechanical coupling between microwave and optical photons, Nat. Phys. **9**, 712 (2013).

[9] R. Andrews, R. W. Peterson, T. Purdy, K. Cicak, R. W. Simmonds, C. A. Regal, and K. W. Lehnert, Bidirectional and efficient conversion between microwave and optical light, Nat. Phys. **10**, 321 (2014).

[10] K. C. Balram, M. I. Davanço, J. D. Song, and K. Srinivasan, Coherent coupling between radiofrequency, optical and acoustic waves in piezo-optomechanical circuits, Nat. Photonics **10**, 346 (2016).

[11] K. Stannigel, P. Rabl, A. S. Sørensen, P. Zoller, and M. D. Lukin, Optomechanical Transducers for Long-Distance Quantum Communication, Phys. Rev. Lett. **105**, 220501 (2010).

[12] C. Dong, Y. Wang, and H. Wang, Optomechanical interfaces for hybrid quantum networks, Natl. Sci. Rev. **2**, 510 (2015).

[13] X. Zhang, C.-L. Zou, L. Jiang, and H. X. Tang, Cavity magnomechanics, Sci. Adv. **2**, e1501286 (2016).

[14] M. F. Colombano, G. Arregui, F. Bonell, N. E. Capuj, E. Chavez-Angel, A. Pitanti, S. O. Valenzuela, C. Sotomayor-Torres, D. Navarro-Urrios, and M. V. Costache, Ferromagnetic Resonance Assisted Optomechanical Magnetometer, Phys. Rev. Lett. **125**, 147201 (2020).

[15] Z. Shen, Y.-L. Zhang, Y. Chen, C.-L. Zou, Y.-F. Xiao, X.-B. Zou, F.-W. Sun, G.-C. Guo, and C.-H. Dong, Experimental realization of optomechanically induced non-reciprocity, Nat. Photonics **10**, 657 (2016).

[16] Z. Shen, Y.-L. Zhang, Y. Chen, F.-W. Sun, X.-B. Zou, G.-C. Guo, C.-L. Zou, and C.-H. Dong, Reconfigurable optomechanical circulator and directional amplifier, Nat. Commun. **9**, 1797 (2018).

[17] A. P. Higginbotham, P. Burns, M. Urmey, R. Peterson, N. Kampel, B. Brubaker, G. Smith, K. Lehnert, and C. Regal, Harnessing electro-optic correlations in an efficient mechanical converter, Nat. Phys. **14**, 1038 (2018).

[18] G. Arnold, M. Wulf, S. Barzanjeh, E. Redchenko, A. Rueda, W. J. Hease, F. Hassani, and J. M. Fink, Converting microwave and telecom photons with a silicon photonic nanomechanical interface, Nat. Commun. **11**, 4460 (2020).

[19] W. Jiang, C. J. Sarabalis, Y. D. Dahmani, R. Patel, F. M. Mayor, T. P. Mckenna, R. Van Laer, and A. H. Safavinaeini, Efficient bidirectional piezo-optomechanical transduction between microwave and optical frequency, Nat. Commun. **11**, 1166 (2020).

[20] M. Forsch, R. Stockill, A. Wallucks, I. Marinkovic, C. Gartner, R. A. Norte, F. W. M. Van Otten, A. Fiore, K. Srinivasan, and S. Groblacher, Microwave-to-optics conversion using a mechanical oscillator in its quantum ground state, Nat. Phys. **16**, 69 (2020).

[21] X. Han, W. Fu, C. Zhong, C.-L. Zou, Y. Xu, A. A. Sayem, M. Xu, S. Wang, R. Cheng, L. Jiang, and H. X. Tang, Cavity piezo-mechanics for superconducting-nanophotonic quantum interface, Nat. Commun. **11**, 3237 (2020).

[22] W. Fu, Z. Shen, Y. Xu, C.-L. Zou, R. Cheng, X. Han, and H. X. Tang, Phononic integrated circuitry and spin–orbit interaction of phonons, Nat. Commun. **10**, 2743 (2019).

[23] D. Lachance-Quirion, S. P. Wolski, Y. Tabuchi, S. Kono, K. Usami, and Y. Nakamura, Entanglement-based single-shot detection of a single magnon with a superconducting qubit, Science **367**, 425 (2020).

[24] N. Zhu, X. Zhang, X. Han, C.-L. Zou, C. Zhong, C.-H. Wang, L. Jiang, and H. X. Tang, Waveguide cavity optomagnonics for microwave-to-optics conversion, Optica **7**, 1291 (2020).

[25] C.-Z. Chai, Z. Shen, Y.-L. Zhang, H.-Q. Zhao, G.-C. Guo, C.-L. Zou, and C.-H. Dong, Single-sideband microwave-to-optical conversion in high-q ferrimagnetic microspheres, Photonics Res. **10**, 820 (2022).

[26] X. Zhang, N. Zhu, C.-L. Zou, and H. X. Tang, Optomagnonic Whispering Gallery Microresonators, Phys. Rev. Lett. **117**, 123605 (2016).

[27] A. Almpanis, *Optomagnonic Structures: Novel Architectures for Simultaneous Control Oflight and Spin Waves* (World Scientific, Singapore, 2021).

[28] B. Z. Rameshti, S. V. Kusminskiy, J. A. Haigh, K. Usami, D. Lachance-Quirion, Y. Nakamura, C.-M. Hu, H. X. Tang, G. E. Bauer, and Y. M. Blanter, Cavity magnonics, Phys. Rep. **979**, 1 (2022).

[29] A. Osada, R. Hisatomi, A. Noguchi, Y. Tabuchi, R. Yamazaki, K. Usami, M. Sadgrove, R. Yalla, M. Nomura, and Y. Nakamura, Cavity Optomagnonics with Spin-Orbit Coupled Photons, Phys. Rev. Lett. **116**, 223601 (2016).

[30] J. Haigh, A. Nunnenkamp, A. Ramsay, and A. Ferguson, Triple-Resonant Brillouin Light Scattering in Magneto-Optical Cavities, Phys. Rev. Lett. **117**, 133602 (2016).

[31] A. Osada, A. Gloppe, R. Hisatomi, A. Noguchi, R. Yamazaki, M. Nomura, Y. Nakamura, and K. Usami, Brillouin Light Scattering by Magnetic Quasivortices in Cavity Optomagnonics, Phys. Rev. Lett. **120**, 133602 (2018).

[32] C.-H. Dong, Z. Shen, C.-L. Zou, Y.-L. Zhang, W. Fu, and G.-C. Guo, Brillouin-scattering-induced transparency and non-reciprocal light storage, Nat. Commun. **6**, 6193 (2015).

[33] G. S. MacCabe, H. Ren, J. Luo, J. D. Cohen, H. Zhou, A. Sipahigil, M. Mirhosseini, and O. Painter, Nano-acoustic resonator with ultralong phonon lifetime, Science **370**, 840 (2020).

[34] A. Wallucks, I. Marinković, B. Hensen, R. Stockill, and S. Gröblacher, A quantum memory at telecom wavelengths, Nat. Phys. **16**, 772 (2020).

[35] C. Dong, V. Fiore, M. C. Kuzyk, and H. Wang, Optomechanical dark mode, Science **338**, 1609 (2012).
[36] See Supplemental Material at http://link.aps.org/supplemental/10.1103/PhysRevLett.129.243601 for details, which includes Refs. [37,38].
[37] V. Fiore, Y. Yang, M. C. Kuzyk, R. Barbour, L. Tian, and H. Wang, Storing Optical Information as a Mechanical Excitation in a Silica Optomechanical Resonator, Phys. Rev. Lett. **107**, 133601 (2011).
[38] V. Fiore, C. Dong, M. C. Kuzyk, and H. Wang, Optomechanical light storage in a silica microresonator, Phys. Rev. A **87**, 023812 (2013).
[39] G.-T. Xu, M. Zhang, Z.-Y. Wang, Y. Wang, Y.-X. Liu, Z. Shen, G.-C. Guo, and C.-H. Dong, Ringing Spectroscopy in the Magnomechanical System, Fundamental Research (to be published).
[40] A. H. Safavi-Naeini, D. V. Thourhout, R. Baets, and R. V. Laer, Controlling phonons and photons at the wavelength scale: integrated photonics meets integrated phononics, Optica **6**, 213 (2019).
[41] E. Gil-Santos, J. J. Ruz, O. Malvar, I. Favero, A. Lemaître, P. M. Kosaka, S. García-López, M. Callejaand, and J. Tamayo, Optomechanical detection of vibration modes of a single bacterium, Nat. Nanotechnol. **15**, 469 (2020).
[42] S. Weis, R. Rivière, S. Deléglise, E. Gavartin, O. Arcizet, A. Schliesser, and T. J. Kippenberg, Optomechanically induced transparency, Science **330**, 1520 (2010).
[43] A. H. Safavi-Naeini, T. M. Alegre, J. Chan, M. Eichenfield, M. Winger, Q. Lin, J. T. Hill, D. E. Chang, and O. Painter, Electromagnetically induced transparency and slow light with optomechanics, Nature (London) **472**, 69 (2011).
[44] Z. Xiang, S. Ashhab, J. Q. You, and F. Nori, Hybrid quantum circuits: Superconducting circuits interacting with other quantum systems, Rev. Mod. Phys. **85**, 623 (2013).
[45] G. Kurizki, P. Bertet, Y. Kubo, K. Molmer, D. Petrosyan, P. Rabl, and J. Schmiedmayer, Quantum technologies with hybrid systems, Proc. Natl. Acad. Sci. U.S.A. **112**, 3866 (2015).